Structural basis for photo-induced protein cleavage and green-to-red conversion of fluorescent protein EosFP

Karin Nienhaus*, G. Ulrich Nienhaus*†‡, Jörg Wiedenmann§, and Herbert Nar¶

Departments of *Biophysics and §General Zoology and Endocrinology, University of Ulm, Albert-Einstein-Allee 11, D-89081 Ulm, Germany; †Department of Physics, University of Illinois at Urbana–Champaign, 1110 West Green Street, Urbana, IL 61801; and ¶Department of Lead Discovery, Boehringer Ingelheim Pharma GmbH & Co. KG, Birkendorfer Strasse 65, D-88397 Biberach/Riss, Germany

Edited by Peter G. Wolynes, University of California at San Diego, La Jolla, CA, and approved May 18, 2005 (received for review March 8, 2005)

Genetically encoded fusion constructs derived from fluorescent proteins (FPs) can be designed to report on a multitude of events and signals in cells, tissues, and entire organs without interfering with the complex machinery of life. EosFP is a novel FP from the scleractinian coral *Lobophyllia hemprichii* that switches its fluorescence emission from green (516 nm) to red (581 nm) upon irradiation with ≈400-nm light. This property enables localized tagging of proteins and thus provides a valuable tool for tracking protein movements within live cells. Here, we present the x-ray structures of the green and red forms of WT EosFP. They reveal that formation of the red chromophore is associated with cleavage of the peptide backbone, with surprisingly little change elsewhere in the structure, and provide insights into the mechanism that generates this interesting posttranslational polypeptide modification.

photochemistry | photoconversion | x-ray structure | Anthozoa

Genetically encoded fusion constructs derived from fluorescent proteins (FPs) can be designed to report on a multitude of events and signals in cells, tissues, and entire organs without interfering with the complex machinery of life. The toolbox of FPs, initially limited to the GFP from the luminescent jellyfish *Aequoria victoria* (1) and its genetically engineered variants (2), has been greatly expanded in recent years by the cloning of FPs from Anthozoa animals. Some of these proteins show exciting new properties, including red-shifted fluorescence (3–7) and photoinducible green-to-red conversion (8–10). The latter property is particularly attractive as it allows regional marking and tracking of proteins in live cells. Unfortunately, the tendency of WT anthozoan FPs to oligomerize often creates problems in fusion constructs so that further optimization by genetic engineering is required (11).

Further advances in FP technology require a detailed understanding of the structural and dynamic processes that accompany photon absorption and emission. The fold topology of GFP features an 11-stranded β-can with a helix in the center (12, 13), in which the chromophore, 4-(*p*-hydroxybenzylidene)-5-imidazolinone, is tightly encased. In GFP, it forms autocatalytically from the tripeptide Ser-Tyr-Gly in an oxidation reaction. Whereas all members of the FP family have an identical overall polypeptide fold (14–17), significant differences can occur in the covalent structure of the chromophore. In red FPs such as DsRed and eqFP611, the GFP chromophore forms initially, and subsequently, the Cα–Nα bond of the first amino acid in the tripeptide oxidizes, thereby extending the π-conjugated electron system along the backbone and shifting the fluorescence emission to the red (5, 7, 15, 18, 19). Green-to-red photoconvertible FPs form another subclass that includes EosFP (9), Kaede (8, 20), DendFP (10), mcavRFP, and rfloRFP (21). They all contain a chromophoric unit that derives from the tripeptide His-Tyr-Gly. In contrast to DsRed and eqFP611, their green-to-red conversion is driven by light rather than chemical oxidation, as it occurs under anaerobic conditions but not in the dark. On the basis of mass spectroscopy and NMR spectroscopy of the red chromophore, Miyawaki and coworkers (20) suggested a model in which the protein moiety catalyzes a β-elimination reaction, thus causing cleavage of the His Nα–Cα bond with concomitant extension of the conjugated π electron system so as to incorporate the imidazole side chain of the histidine into the chromophore. Clearly, such a scenario depends on the precise stereochemical alignment of the groups involved in this reaction. Consequently, elucidation of this peculiar posttranslational modification requires knowledge of the overall structure of the polypeptide moiety and the chromophore. Here, we present the x-ray structures of both the green and red forms of EosFP at 1.85 and 2.0 Å, respectively. The crystallographic analysis is summa-

Table 1. Summary of crystallographic analysis

	Green species	Red species
Data collection statistics		
Space group	$P2_12_12_1$	$P2_12_12_1$
a, Å	73.3	70.6
b, Å	106.5	105.5
c, Å	121.5	119.6
Resolution, Å	1.85	2.0
Total observations	319,519	342,041
Unique reflections	79,379	60,658
Completeness, %	97.3 (78.2)	99.9 (100.0)
R_{merge}, %*	4.8 (41.2)	7.7 (43.5)
$I/\sigma(I)$	11.8 (4.2)	13.2 (5.5)
Refinement		
R_{cryst}, %	21.1	19.8
R_{free}, %	24.2	23.1
No. of protein atoms	7,104	7,104
No. of waters	632	696
rms deviation from ideality		
Bond lengths, Å	0.006	0.006
Bond angles, °	1.40	1.37
Average *B* factors, Å^2		
All atoms	27.5	27.2
Chromophore	24.2	23.2
rmsd bonded *B*, Å^2	0.40	0.52

Numbers in parentheses refer to the highest-resolution shell (2.0–1.85 Å for the green species, 2.1–2.0 Å for the red species).

*$R_{merge} = \Sigma_{hkl}\,\Sigma_j|I_j(hkl) - \langle I(hkl)\rangle|/\Sigma_{hkl}\,\Sigma_j\,\langle I(hkl)\rangle$, with $I_j(hkl)$ representing the intensity of measurement *j* and $\langle I(hkl)\rangle$ the mean of measurements for the reflection *hkl*.

This paper was submitted directly (Track II) to the PNAS office.

Abbreviation: FP, fluorescent protein.

Data deposition: The atomic coordinates and structure factors have been deposited in the Protein Data Bank, www.pdb.org (PDB ID codes 2BTJ and 1ZUX).

‡To whom correspondence should be addressed. E-mail: uli@uiuc.edu.

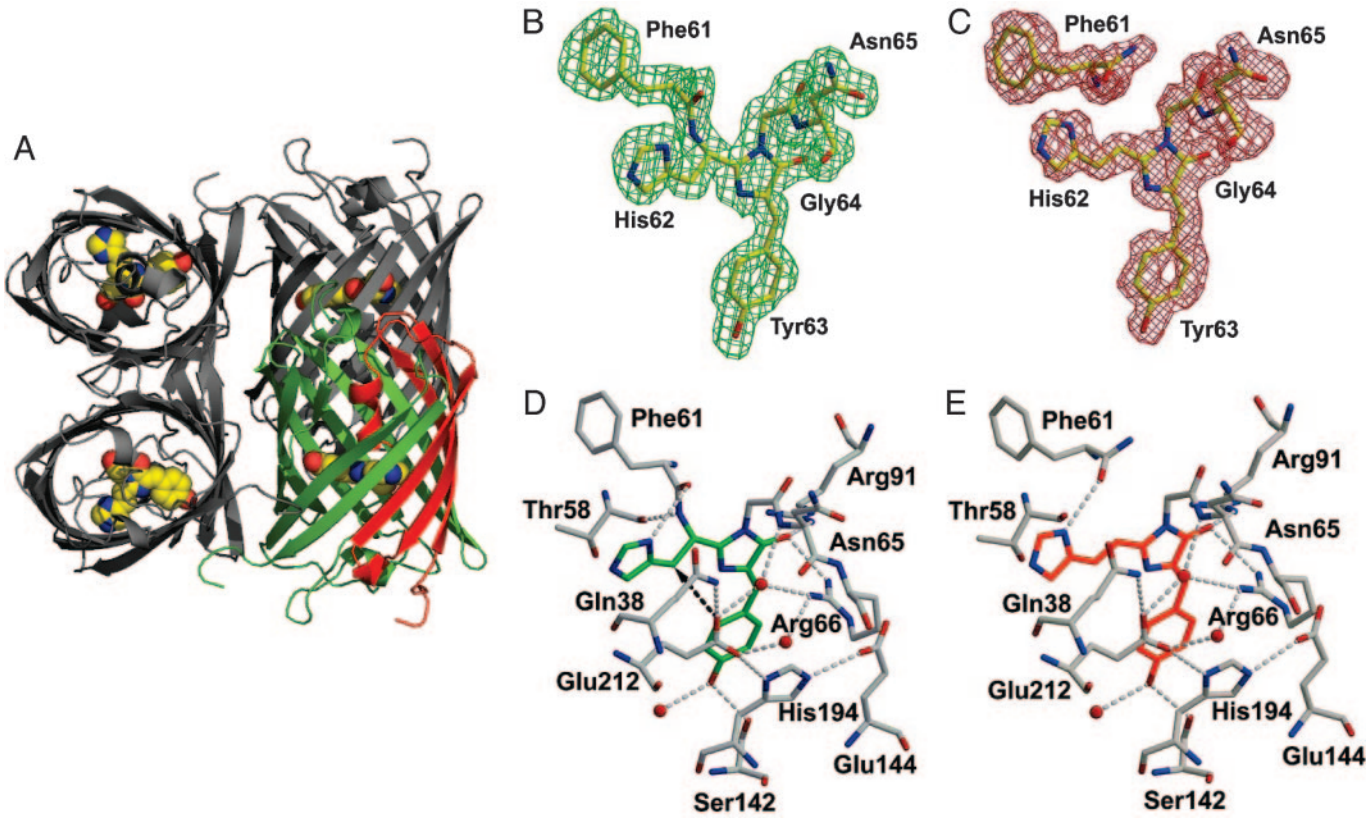

Fig. 1. Molecular structure of EosFP. (*A*) Ribbon diagram of the EosFP tetramer. For one of the monomers, green and red colors indicate the protein fragments created by photoconversion. The atoms in the chromophore are color-coded. (*B* and *C*) The electron densities (2 F_o − Fc) of the green (*B*) and red (*C*) chromophores are contoured at 1.2 σ. (*D* and *E*) The hydrogen bonds constraining the green (*D*) and red (*E*) chromophores are represented by dashed lines. The dashed arrow depicts the interaction between the Glu-212 carboxyl and His-62 Cβ–H that is essential for cleavage of the His-62 Nα–Cα bond.

rized in Table 1. Based on inspection of the chromophores and their immediate environments, we propose a mechanism for the light-induced conversion process.

Materials and Methods

Crystallization. EosFP was expressed in *Escherichia coli* (strain M15pREP4) and purified as described (9). Crystals were grown at 20°C in 30% PEG 4000, 0.1 M Tris, 0.2 M sodium acetate (pH 8.5), using the hanging drop vapor diffusion method. After a few days, small pyramidal crystals appeared that reached a final size of 0.15 mm^3 after ≈1 week. Great care was taken to set up the crystallization trials of the green species in the dark. The crystals were transferred to cryosolvent (10% glycerol/30% PEG 4000/0.1 M Tris, pH 8.5/0.2 M sodium acetate) and flash-frozen in liquid nitrogen.

X-Ray Structure Analysis. Data sets were collected at 100 K on a MAR345dtb image plate detector (MAR-Research, Hamburg) using radiation from a RU300 x-ray generator (Rigaku, Houston) equipped with Osmic confocal optics (Rigaku). Reflection data were integrated and scaled with HKL (22).

The structure of red EosFP was solved by molecular replacement with the program PHASER (23, 24) using coordinates of *Montipora efflorescens* chromoprotein Rtms5 (Protein Data Bank ID code 1MOV) (25), which exhibits 50% sequence identity to EosFP. A search model was constructed by omitting the chromophore and residues differing between the two proteins. Model building and crystallographic refinement were performed with MAIN (26) and CNX (27, 28). Initially, coordinates of the individual subunits of the tetramer were kept identical in the refinement. In later stages, noncrystallographic symmetry restraints were removed.

The structure of the green form of EosFP was determined by molecular replacement with the program AMORE (29) by using the refined coordinates of the red form as a search model. Simple rigid body refinement of the individual monomers of red EosFP did not result in the correct structure of the green form of the functional protein complex.

For both forms, chromophores were modeled in the later stages of refinement. From the difference electron density maps, it was immediately obvious that the green form had an intact amide bond between residues Phe-61 and His-62, whereas the red form clearly showed a break in the backbone between these residues. The electron density of the red form confirmed a carboxamide structure at Phe-61 (Fig. 1*C*).

The refined models for both forms of EosFP consist of tetramers of EosFP subunits and a large number of well ordered water molecules. The electron density defines residues Ile-4 to Asp-222 of the expressed protein sequence; both models exhibit excellent stereochemistry.

Results and Discussion

Overall Structure. Fig. 1*A* gives an overall view of the EosFP structure showing the arrangement of dimers of dimers typical of anthozoan FPs (14–16). A comparison of the green and red EosFP structures shows that, with the exception of residues Phe-61 and His-62, the chromophore, its environment, and even the water structure around the chromophore are entirely unperturbed by the photochemical modification. The conservation of the 3D structure is reflected by the overall rms displacements

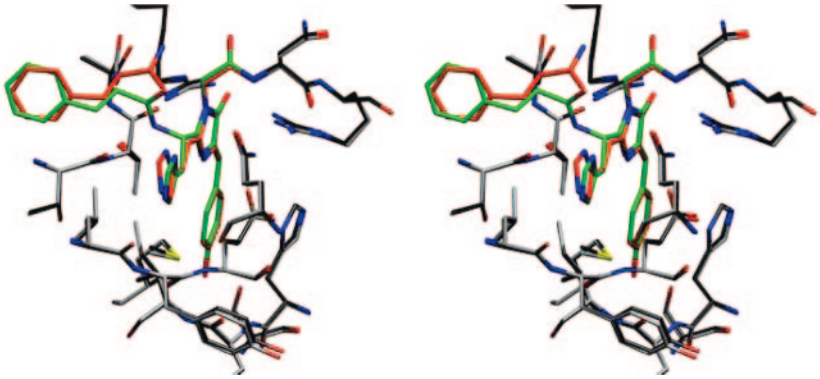

Fig. 2. Stereo diagram of EosFP in the vicinity of the chromophore. Carbon atoms are shown in green/black and red/gray for the green and red forms, respectively. Except for residues Phe-61 and His-62, the protein structures superimpose almost perfectly, indicating surprisingly little change in the overall structure.

for the Cα atoms of 0.25 Å between the green and red monomers and the respective tetramers.

Structure of Green EosFP. In its anionic form, the green chromophore in EosFP exhibits absorption and emission maxima at 506 and 516 nm, respectively. It forms autocatalytically from amino acids His-62, Tyr-63, and Gly-64 and features the typical 4-(*p*-hydroxybenzylidene)-5-imidazolinone moiety. Its chemical structure is very well established in the electron density (Fig. 1*B*). Crystallographic refinement reveals an almost perfectly planar chromophore structure, with torsion angles around the two exocyclic bonds of 4° and 8°. A cluster of charged or polar amino acids and structural water molecules are visible in the immediate vicinity of the chromophore (Fig. 1*D*). Both Arg-66 and Arg-91 engage in hydrogen bonds to the carbonyl oxygen of the imidazolinone moiety. A close-knit network of hydrogen bond interactions between Glu-144, His-194, Glu-212, and Gln-38 is located above the plane of the chromophore. The Thr-58 backbone carbonyl is hydrogen-bonded to the backbone NH of His-62. The His-62 side chain adopts an extended conformation (ψ = 168°; χ_1 = 167°) and resides in an unpolar environment. Whereas its Nε nitrogen is left without polar interactions, its Nδ–H group forms a contact to the preceding backbone carbonyl oxygen of Phe-61 at a distance of 3.3 Å. Particularly interesting with respect to the mechanism of light-induced backbone cleavage is the observation that one of the carboxylate oxygens of Glu-212 is positioned only 3.3 Å away from His-62–Cβ.

Structure of Red EosFP. The red chromophore in EosFP, with absorption and emission maxima at 571 and 581 nm, respectively, in its anionic form (9), is unequivocally defined by the experimental data (Fig. 1*C*). It is generated by cleavage of the peptide backbone, as was already suggested from our gel electrophoresis studies that showed two subfractions of 8 and 20 kDa (9). The break occurs between His-62 Nα and Cα, as inferred by Mizuno *et al.* (20). The electron density at Phe-61 is consistent with a carboxamide structure. The observed red-shifted absorption and fluorescence results from an extension of the π-conjugation of the chromophore, by which the His-62 imidazole ring system connects to the imidazolinone via an *all-trans* alkenylene structure (Fig. 1*E*). Slight structural adjustments of the 3-carbon bridge and the imidazole ring upon photoconversion result in a conjugation of the 2-[(1*E*)-2-(5-

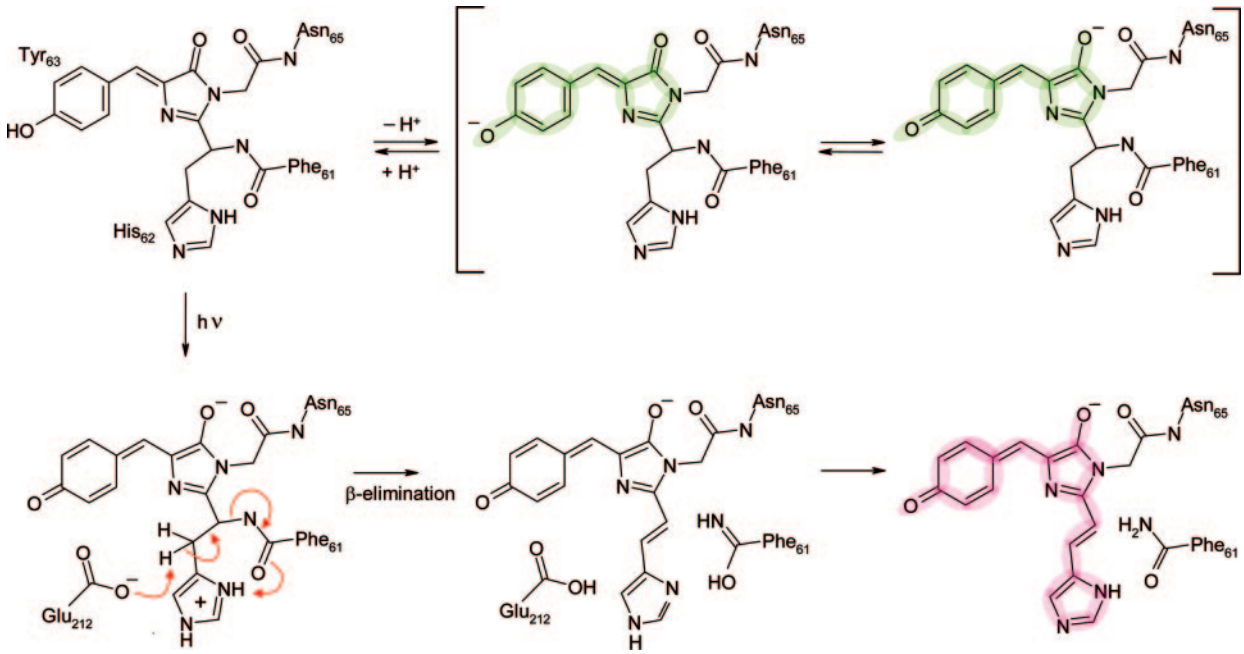

Fig. 3. Reaction mechanism explaining chromophore extension and backbone cleavage. Details are discussed in the text.

imidazolyl)ethenyl] and the 4-(*p*-hydroxybenzylidene)-5-imidazolinone moieties. As already observed in the green structure, the carbonyl oxygen of Phe-61 is hydrogen-bonded to the Nδ–H of the His-62 imidazole. Comparison of Fig. 1 *D* and *E* shows that the hydrogen bond patterns are almost identical for the two forms. Superposition of the green and red structure in the vicinity of the chromophore underscores the similarity of both species (Fig. 2), which is surprising in light of the drastically changed photophysical properties.

Photochemical Conversion Mechanism. The x-ray structures presented here enable us to discuss the details of the green-to-red conversion mechanism, considering interactions between the chromophoric unit and the residues in its vicinity. To explain cleavage of the His-62–Nα–Cα bond, we note that Glu-212 is poised to function as a base that may abstract a proton from His-62–Cβ. The observation that replacement of Glu-212 by glutamine abolishes photoconversion (data not shown) underscores the key role of this residue. The conformation of His-62 is preformed for an E2-type β-elimination reaction, with Glu-212 acting as the nucleophile attacking one of the two His-62–Cβ protons positioned trans to a carboximidic acid leaving group that subsequently changes into its preferred carboxamide tautomeric form (Fig. 3). The proposed mechanism does not yet involve photoexcitation, which is known to play a key role in the conversion. Two experimental observations are crucial: the yield of photoconversion of EosFP increases drastically at low pH, in proportion to the fraction of molecules in the protonated form, and moreover, the action spectrum for photoconversion has been observed to track the absorption spectrum of the protonated form (9). Both of these observations strongly suggest that the neutral form of the green chromophore, with a protonated Tyr-63 phenyl side chain (pK ≈5.8) and an absorbance peak at ≈390 nm, is the gateway structure for photoconversion of EosFP (Fig. 3). In GFP, efficient fluorescence is not only observed upon excitation of the anionic form but also of the neutral form because of deprotonation of the phenyl group in the excited state (30, 31). EosFP, by contrast, shows strongly decreasing fluorescence toward low pH, indicating that this deprotonation mechanism is suppressed. Still, we propose that proton ejection from the Tyr-63 phenyl side chain is a crucial event in our conversion mechanism, keeping in mind that photoconversion is a process with fairly small quantum yield (9). The proton is subsequently transferred to the His-62 imidazole, which is observed to be hydrogen-bonded with its Nδ–H to the Phe-61 carbonyl in both the green and red forms. An additional proton on Nε increases the tendency of the His-62 Nδ–H to donate its proton to the Phe-61 carbonyl, thus rendering the peptide group between Phe-61 and His-62 an ideal carboximidic leaving group in the elimination reaction. After backbone cleavage, the proton on the Phe-61 carbonyl rearranges to form the carboxamide, and the imidazole tautomerizes so as to reform the H-bond between the Phe-61 carbonyl and His-62 Nδ–H. Consequently, His-62 is an essential group in the proposed mechanism, which is underscored by the observation that EosFP loses its photoconversion ability after replacement of His-62 by other amino acids (9). Finally, as previously suggested by Mizuno *et al.* (20), the internal charge distribution of the green chromophore changes upon photoexcitation so as to further assist in the elimination reaction.

Conclusions

The x-ray structures presented here provide details on the stereochemical interactions of the chromophore with the surrounding protein matrix. These data have enabled us to propose a mechanism for photo-induced green-to-red conversion. Cleavage of the His-62–Nα–Cα bond creates the red 2-[(1*E*)-2-(5-imidazolyl)ethenyl]-4-(*p*-hydroxybenzylidene)-5-imidazolinone chromophore in a β-elimination reaction, in which Glu-212 acts as a base for proton abstraction from His-62–Cβ, whereas the His-62 side chain, which is transiently protonated because of photoexcitation, simultaneously assists in the reaction by donating a proton to the Phe-61 carbonyl in the leaving group. It is impressive to see how this intricate covalent chemistry takes place in the interior of the EosFP β-can without creating any other changes in the protein structure.

We thank Uwe Theilen for protein expression and purification. This work was supported by Deutsche Forschungsgemeinschaft Grants SFB 569 and GRK 328 and the Fonds der Chemischen Industrie.

1. Prasher, D. C., Eckenrode, V. K., Ward, W. W., Prendergast, F. G. & Cormier, M. J. (1992) *Gene* **111,** 229–233.
2. Tsien, R. Y. (1998) *Annu. Rev. Biochem.* **67,** 509–544.
3. Matz, M. V., Fradkov, A. F., Labas, Y. A., Savitsky, A. P., Zaraisky, A. G., Markelov, M. L. & Lukyanov, S. A. (1999) *Nat. Biotechnol.* **17,** 969–973.
4. Wiedenmann, J., Elke, C., Spindler, K. D. & Funke, W. (2000) *Proc. Natl. Acad. Sci. USA* **97,** 14091–14096.
5. Wiedenmann, J., Schenk, A., Röcker, C., Girod, A., Spindler, K. D. & Nienhaus, G. U. (2002) *Proc. Natl. Acad. Sci. USA* **99,** 11646–11651.
6. Schenk, A., Ivanchenko, S., Röcker, C., Wiedenmann, J. & Nienhaus, G. U. (2004) *Biophys. J.* **86,** 384–394.
7. Wiedenmann, J., Vallone, B., Renzi, F., Nienhaus, K., Ivanchenko, S., Röcker, C. & Nienhaus, G. U. (2005) *J. Biomed. Opt.* **10,** 14003.
8. Ando, R., Hama, H., Yamamoto-Hino, M., Mizuno, H. & Miyawaki, A. (2002) *Proc. Natl. Acad. Sci. USA* **99,** 12651–12656.
9. Wiedenmann, J., Ivanchenko, S., Oswald, F., Schmitt, F., Röcker, C., Salih, A., Spindler, K. D. & Nienhaus, G. U. (2004) *Proc. Natl. Acad. Sci. USA* **101,** 15905–15910.
10. Pakhomov, A. A., Martynova, N. Y., Gurskaya, N. G., Balashova, T. A. & Martynov, V. I. (2004) *Biochemistry (Moscow)* **69,** 901–908.
11. Shaner, N. C., Campbell, R. E., Steinbach, P. A., Giepmans, B. N., Palmer, A. E. & Tsien, R. Y. (2004) *Nat. Biotechnol.* **22,** 1567–1572.
12. Ormö, M., Cubitt, A. B., Kallio, K., Gross, L. A., Tsien, R. Y. & Remington, S. J. (1996) *Science* **273,** 1392–1395.
13. Yang, F., Moss, L. G. & Phillips, G. N. (1996) *Nat. Biotechnol.* **14,** 1246–1251.
14. Wall, M. A., Socolich, M. & Ranganathan, R. (2000) *Nat. Struct. Biol.* **7,** 1133–1138.
15. Yarbrough, D., Wachter, R. M., Kallio, K., Matz, M. V. & Remington, S. J. (2001) *Proc. Natl. Acad. Sci. USA* **98,** 462–467.
16. Nienhaus, K., Vallone, B., Renzi, F., Wiedenmann, J. & Nienhaus, G. U. (2003) *Acta Crystallogr. D* **59,** 1253–1255.
17. Petersen, J., Wilmann, P. G., Beddoe, T., Oakley, A. J., Devenish, R. J., Prescott, M. & Rossjohn, J. (2003) *J. Biol. Chem.* **278,** 44626–44631.
18. Verkhusha, V. V. & Lukyanov, K. A. (2004) *Nat. Biotechnol.* **22,** 289–296.
19. Verkhusha, V. V., Chudakov, D. M., Gurskaya, N. G., Lukyanov, S. & Lukyanov, K. A. (2004) *Chem. Biol.* **11,** 845–854.
20. Mizuno, H., Mal, T. K., Tong, K. I., Ando, R., Furuta, T., Ikura, M. & Miyawaki, A. (2003) *Mol. Cell* **12,** 1051–1058.
21. Shagin, D. A., Barsova, E. V., Yanushevich, Y. G., Fradkov, A. F., Lukyanov, K. A., Labas, Y. A., Semenova, T. N., Ugalde, J. A., Meyers, A., Nunez, J. M., *et al.* (2004) *Mol. Biol. Evol.* **21,** 841–850.
22. Gewirth, D. (1994) *The HKL Manual* (Yale University, New Haven, CT).
23. Read, R. J. (2001) *Acta Crystallogr. D* **57,** 1373–1382.
24. Storoni, L. C., McCoy, A. J. & Read, R. J. (2004) *Acta Crystallogr. D* **60,** 432–438.
25. Beddoe, T., Ling, M., Dove, S., Hoegh-Guldberg, O., Devenish, R. J., Prescott, M. & Rossjohn, J. (2003) *Acta Crystallogr. D* **59,** 597–599.
26. Turk, D. (1992) Thesis (Technical University, Munich).
27. Engh, R. A. & Huber, R. (1991) *Acta Crystallogr. A* **47,** 392–400.
28. Bruenger, A. T., Adams, P. D., Clore, G. M., DeLano, W. L., Gros, P., Grosse-Kunstleve, R. W., Jiang, J. S., Kuszewski, J., Nilges, M., Pannu, N. S., *et al.* (1998) *Acta Crystallogr. D* **54,** 905–921.
29. Navaza, J. (1994) *Acta Crystallogr. A* **50,** 157–163.
30. Lossau, H., Kummer, A., Heinecke, R., Pollinger-Dammer, F., Kompa, C., Bieser, G., Jonsson, T., Silva, C. M., Yang, M. M., Youvan, D. C. & Michel-Beyerle, M. E. (1996) *Chem. Phys.* **213,** 1–16.
31. Chattoraj, M., King, B. A., Bublitz, G. U. & Boxer, S. G. (1996) *Proc. Natl. Acad. Sci. USA* **93,** 8362–8367.